ISSN 1054-660X, Laser Physics, 2006, Vol. 16, No. 10, pp. 1478–1485.

Robustness of Optimal Working Points for Nonadiabatic Holonomic Quantum Computation

A. Trullo[a], P. Facchi[b, c], R. Fazio[d, e], G. Florio[a, c], V. Giovannetti[d], and S. Pascazio[a, c, *]

[a] *Dipartimento di Fisica, Università di Bari, Bari, I-70126 Italy*
[b] *Dipartimento di Matematica, Università di Bari, Bari, I-70125 Italy*
[c] *INFN, Sezione di Bari, Bari, I-70126 Italy*
[d] *NEST-CNR-INFM and Scuola Normale Superiore, Pisa, I-56126 Italy*
[e] *International School for Advanced Studies (SISSA), Trieste, I-34014 Italy*
*e-mail: saverio.pascazio@ba.infn.it
Received May 23, 2006

Abstract—Geometric phases are an interesting resource for quantum computation in view of their robustness against decoherence effects. We study the effects of the environment on a class of one-qubit holonomic gates that have recently been shown to be characterized by "optimal" working times. We numerically analyze the behavior of these optimal points and focus on their robustness against noise.

PACS numbers: 03.67.Lx; 03.65.Yz; 03.65.Vf

DOI: 10.1134/S1054660X06100094

1. INTRODUCTION

Quantum algorithms based on geometric phases [1, 2] are attracting increasing interest in quantum computation [3, 4]. The related quantum gates representing the unitary transformations on a register of qubits do not have a dynamical origin: the Hamiltonian depends on time through a set of control parameters that change by following suitable closed loops in the associated parameter space; in the adiabatic limit, the dynamical contribution to the evolution can be factorized, and the features of the quantum gate depend only on the topological structure of the manifold.

Geometric quantum computation has been investigated using both Abelian [5] and non-Abelian [6] holonomies. There have been several proposals for their implementation using ion traps [7], Josephson junctions [8, 9], and semiconductors [10]. Since all physical devices interact with their environment, one must carefully analyze the onset of decoherence [11] and its detrimental effects against realistic implementations of quantum gates and algorithms. In particular, the effects of noise for non-Abelian holonomies in open quantum systems have been recently investigated in a series of articles [12–16]. In [14], we studied a class of one-qubit gates implemented on a four-level ("tripod") system [7], focusing on nonadiabatic effects and bringing to light the presence of fidelity revivals, namely, an infinite number of (optimal) times at which the fidelity reaches unity.

In this article, we shall investigate the behavior of the fidelity at the first of these optimal working points and study its robustness against noise effects. The deviations from the ideal (noiseless) case will be numerically analyzed as a function of the strength of the noise (the coupling of the system with its environment) and a heuristic definition on robustness will be introduced.

This paper is organized as follows. We review the concept of holonomy in Section 2 and briefly introduce the specific tripod system [7] in Section 3, where we focus on the role of nonadiabatic effects. In Section 4, we outline the main features of the master equation for time-dependent Hamiltonians; this is numerically solved in Section 5 in order to analyze the behavior of the optimal working points in the presence of noise. In Section 6, we conclude and discuss the robustness of our gates.

2. ABELIAN AND NON-ABELIAN HOLONOMIES

We consider a system governed by a nondegenerate Hamiltonian that depends on time through a set of parameters, adiabatically covering a closed loop in the parameter space. Under these conditions, the final state exhibits, in addition to the dynamical phase, also a geometric phase, whose structure depends only on the topological properties of the parameter manifold [19]. If the Hamiltonian has some degeneracies, a loop in the parameter space involves more complex geometric transformations [20]. We suppose that the family of Hamiltonians $H(x(t))$ ($x^{\mu}(t)$ being a set of parameters) is iso-degenerate, i.e., that the dimensions of its eigenspaces do not depend on the parameters and the eigenprojections $P_m(x(t))$ (m denoting the eigenvalue) have a smooth dependence on t (at least twice continuously differentiable). In particular, this entails the absence of level crossings between different eigenspaces. $H(t)$ can be decomposed by using its instantaneous eigenprojec-

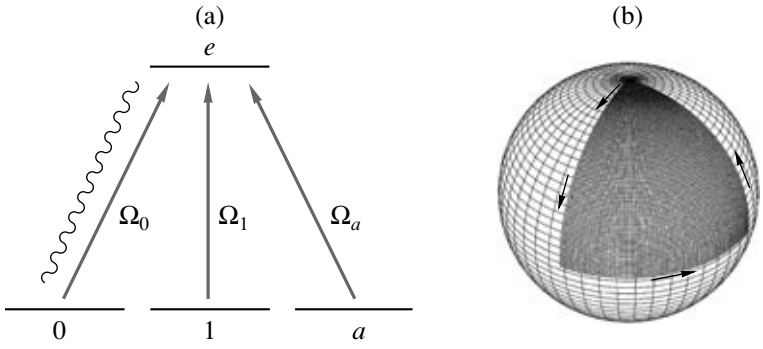

Fig. 1. (a) Scheme of a tripod system. 0 and 1 are the computational levels, while a is an ancilla state used for the intermediate steps of the transformation. The three degenerate levels are connected with an upper level e by time-dependent Rabi frequencies $\Omega_j(t)$. The wavy line represents the noise, which induces additional transitions only between 0 and e. (b) Path in parameter space for the realization of a NOT gate. The solid angle spanned during the evolution is $\pi/2$.

tions $H(t) = \sum_m \epsilon_m(t) P_m(t)$, with $P_m(t) = \sum_k |m_k(t)\rangle\langle m_k(t)|$ and k the degeneracy index. We define the operator R, which transports every eigenprojection from t_0 to t, and its Hermitian generator $D(t, t_0)$,

$$\begin{aligned} R(t, t_0)P_m(t_0) &= P_m(t)R(t, t_0), \\ D(t, t_0) &= -iR(t, t_0)^\dagger \frac{\partial}{\partial t} R(t, t_0). \end{aligned} \tag{2.1}$$

In the adiabatic limit, the evolution of the state remains confined to the degenerate eigenspaces, and the evolution operator U becomes block-diagonal. In the case of cyclic evolution ($P_m(t) = P_m(t_0)$),

$$\begin{aligned} U(t, t_0) &\sim \sum_m P_m(t_0) e^{-i\int_{t_0}^{t} \epsilon_m(s)ds} U^m_{\mathrm{ad}} P_m(t_0), \\ U^m_{\mathrm{ad}} &= \mathbf{P}\exp\left\{-\oint_C A^m(x)\right\}, \end{aligned} \tag{2.2}$$

and the geometric evolution is given by a path-ordered integral ($\mathbf{P}$ in the above formula) of the adiabatic connection $A^m(x) = \sum_\mu A^m_\mu dx^\mu$, with

$$\begin{aligned} A^m_\mu(x(t)) &= P_m(x(t_0))R^\dagger(x(t), x(t_0)) \\ &\times \frac{\partial}{\partial x^\mu} R(x(t), x(t_0))P_m(x(t_0)). \end{aligned} \tag{2.3}$$

If the eigenvalues ϵ_m are time-independent and the connection D is piecewise-constant (i.e., $D(t, t_0) = D(t_0, t_0)$ $\forall s \in [t, t_0]$), the evolution operator reduces to the useful expression [14]

$$U(t, t_0) = e^{i(t-t_0)D(t_0, t_0)} e^{-i(t-t_0)(H(t_0) + D(t_0, t_0))}. \tag{2.4}$$

We will study a large class of gates where the above hypotheses are satisfied and one can exactly evaluate the time evolution, including all nonadiabatic effects, by making use of expression (2.4).

3. FREE IDEAL EVOLUTION

We focus on the "tripod" system introduced in [7] for holonomic quantum computation; see Fig. 1a, where three degenerate levels are connected with a fourth by Rabi oscillations. The adiabatic evolution of this system was analyzed in several articles for different experimental implementations [7, 9, 10]. Let us first review the ideal noiseless case, taking into account also nonadiabatic effects. At time $t = 0$, the logical states 0 and 1 are encoded respectively in the quantum states $|0\rangle$ and $|1\rangle$, while $|a\rangle$ is an ancilla state used as "buffer" during the evolution. The Hamiltonian of the system is $H(t) = |e\rangle(\Omega_0(t)\langle 0| + \Omega_1(t)\langle 1| + \Omega_a(t)\langle a|) + \mathrm{H.c.}$, where $\Omega_j(t)$ represents the time-dependent Rabi frequencies of the transitions. The loop in the parameter space is obtained by varying $\Omega_j(t)$ ($j = 0, 1, a$). In our calculations, we consider $\Omega_j(t) \in \mathbf{R}$, $\forall t$. The eigenvalues of the system are $\{0, \pm\sqrt{\Omega_0(t)^2 + \Omega_1(t)^2 + \Omega_a(t)^2} = \pm\Omega\}$, where 0 is 2-fold-degenerate, corresponding to a two-dimensional (computational) eigenspace, and Ω is kept constant. Therefore, the parameter space is the 2-sphere of radius Ω, $\{\Omega_j \in \mathbf{R} | \sum_j \Omega_j^2 = \Omega^2\}$, shown in Fig. 1b. Introducing the parametrization

$$\begin{aligned} \Omega_1 &= \Omega\sin\vartheta\cos\varphi, \quad \Omega_0 = \Omega\sin\vartheta\sin\varphi, \\ \Omega_a &= \Omega\cos\vartheta, \end{aligned} \tag{3.1}$$

the eigenstates take the form

$$\begin{aligned} |D_0(t)\rangle &= \cos\varphi|0\rangle - \sin\varphi|1\rangle, \\ |D_1(t)\rangle &= \cos\vartheta\sin\varphi|0\rangle + \cos\vartheta\cos\varphi|1\rangle - \sin\vartheta|a\rangle, \\ |D_\pm(t)\rangle &= (\pm|e\rangle + \sin\vartheta\sin\varphi|0\rangle \\ &\quad + \sin\vartheta\cos\varphi|1\rangle + \cos\vartheta|a\rangle)/(\sqrt{2}). \end{aligned} \tag{3.2}$$

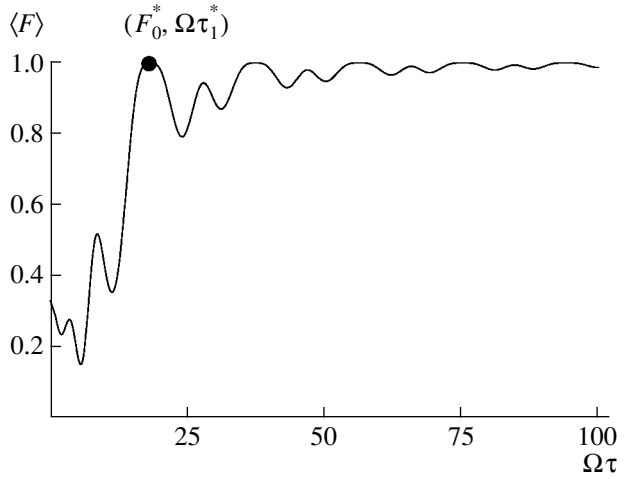

Fig. 2. Mean fidelity versus the cyclic time $\Omega\tau$ (noiseless case). Ω is the energy gap between the bright and dark states. τ is the time needed to cover the loop shown in Fig. 1b. The average is performed over a set of initial states uniformly distributed on the Bloch sphere. The dot on the first significant peak indicates the optimal working point, $F_0^* = 1$ and $\Omega\tau_1^* = 18.25$.

The computational space $C_S = \mathrm{Span}\{|D_0(t)\rangle, |D_1(t)\rangle\}$ belongs to the degenerate eigenvalue 0, while $|D_\pm(t)\rangle$ are the bright eigenstates belonging to $\pm\Omega$. One easily shows that, for a closed loop on the 2-sphere in the computational space, the holonomy (2.2) is $U_{\mathrm{ad}} = \exp(i\sigma_y\omega)$, where $\sigma_y = -i(|D_0(t_0)\rangle\langle D_1(t_0)| - |D_1(t_0)\rangle\langle D_0(t_0)|)$ and ω is the solid angle enclosed by the loop. In particular, if $\omega = \pi/2$, we have $U_{\pi/2} = \exp(i\sigma_y\pi/2) = i\sigma_y$ (in the basis $\{|D_0(t_0)\rangle, |D_1(t_0)\rangle\}$), which represents a NOT transformation (up to a phase for the state $|D_0\rangle$).

Following the discussion of the previous section, we discuss the nonadiabatic corrections to this system. In order to use Eq. (2.4), we will consider the loop shown in Fig. 1b, enclosing the solid angle $\pi/2$; in the adiabatic limit (when $\Omega\tau \longrightarrow \infty$, where τ is the total time of the cyclic evolution and Ω is the energy of the bright states), this path yields a NOT gate. The first step consists in constructing the operator D from Eq. (3.2) and definition (2.1). One can see [14] that, as far as the rate of change of the polar angles is constant in each section of the path, $D(t, t_0)$ is piecewise-constant and we can use Eq. (2.4) to evaluate the evolution operator along the path shown in Fig. 1b.

An interesting feature of the evolution is that it is factorized in three terms. In the adiabatic limit, it simplifies to

$$U_{\pi/2}(\Omega\tau) = U_3(\Omega\tau_3)U_2(\Omega\tau_2)U_1(\Omega\tau_1) \xrightarrow{\tau\Omega\to\infty} U^{\mathrm{ad}}_{\pi/2}(\Omega\tau)$$
$$= \begin{pmatrix} 0 & 1 & 0 & 0 \\ -1 & 0 & 0 & 0 \\ 0 & 0 & e^{-i\tau\Omega} & 0 \\ 0 & 0 & 0 & e^{+i\tau\Omega} \end{pmatrix}, \quad (3.3)$$

where τ is the total evolution time needed to cover the loop in the parameter space and $\tau_i = \alpha_i\tau$, with $\sum_i \alpha_i = 1$. This represents a NOT gate for the degenerate subspace and yields (fast oscillating) dynamical phases for the bright states.

In order to understand how close the evolution operator is to the ideal one, we use the mean fidelity

$$\langle F\rangle(\Omega\tau) = \frac{1}{4\pi}\int d\cos\vartheta d\varphi F(\Omega\tau, \vartheta, \varphi)$$
$$= \frac{1}{4\pi}\int d\cos\vartheta d\varphi\, \mathrm{Tr}\{\sigma_{\mathrm{ad}}(\Omega\tau, \vartheta, \varphi)\sigma(\Omega\tau, \vartheta, \varphi)\}, \quad (3.4)$$

where

$$\sigma(\Omega\tau, \vartheta, \varphi) = U_{\pi/2}(\Omega\tau)\sigma(\vartheta, \varphi)U^{\dagger}_{\pi/2}(\Omega\tau), \quad (3.5)$$

$$\sigma_{\mathrm{ad}}(\Omega\tau, \vartheta, \varphi) = U^{\mathrm{ad}}_{\pi/2}(\Omega\tau)\sigma(\vartheta, \varphi)U^{\mathrm{ad}\dagger}_{\pi/2}(\Omega\tau), \quad (3.6)$$

$\sigma(\vartheta, \varphi) = |\vartheta, \varphi\rangle\langle\vartheta, \varphi|$ being the initial state (assumed to be pure). In practice, in our analysis, F will always be averaged over a finite set of input states uniformly distributed on the Bloch sphere. The mean fidelity is plotted in Fig. 2 as a function of the adiabaticity parameter $\Omega\tau$. Clearly, $\langle F\rangle$ asymptotically approaches unity (with some oscillations), as expected (adiabatic limit). Notice that the fidelity is exactly one for some *finite* values of time, $\tau = \tau_k^*$, which are independent of the initial state. In this case, the NOT transformation is perfect, even though one is far from the adiabatic regime.

It is possible to show that, when the three arcs in the loop in Fig. 1b are covered in equal times, one obtains

$$\tau_k^* = \frac{3\pi}{2\Omega}\sqrt{16k^2 - 1}, \quad k \in \mathbf{N}^*. \quad (3.7)$$

The first fidelity revival occurs for $k = 1$,

$$\Omega\tau_1^* = \frac{3\pi}{2}\sqrt{15} = 18.25, \quad (3.8)$$

and is indicated by a dot in Fig. 2. These revivals (the first one in particular) can be important for experimental applications: in principle, they would enable one to obtain a perfect NOT transformation without reaching the adiabatic regime. It is important to notice that this result does not depend on the initial state of the system but is a feature of the chosen path (see [14] for details).

Finally, we emphasize that similar features (and in particular the presence of the revivals in the nonadiabatic regime) hold for a large class of gates. For transformations consisting in a loop that starts at the pole and is composed of three geodesics given by two arcs of meridians and an arc of the equator enclosing a solid angle $\omega = \pi/2n$ ($n \in \mathbf{N}^*$), there is a straightforward generalization of Eq. (3.7):

$$\tau_k^*(n) = \frac{(2n+1)\pi}{2n\Omega}\sqrt{16k^2n^2 - 1}. \quad (3.9)$$

This expression is valid provided that the loop is covered at a constant angular speed (see Fig. 1b): $\dot{\vartheta}_{arc1} = \dot{\varphi}_{arc2} = \dot{\vartheta}_{arc3} = \text{const}$. Reversing the orientation of the loop leads to identical results.

4. MASTER EQUATION FOR A TIME-DEPENDENT HAMILTONIAN

The interaction between a system and the environment is usually analyzed in terms of a master equation. In the standard approach to this problem, one assumes that the Hamiltonian of the system is time-independent (see, for instance, [21]). For time-dependent Hamiltonians, a slightly different approach is needed [14, 22]. We consider a general Liouville operator with a time-dependent system Liouvillian

$$\begin{aligned}\mathcal{L}(t) &= \mathcal{L}_0(t) + \lambda\mathcal{L}_{SB} \\ &= \mathcal{L}_S(t) \otimes 1 + 1 \otimes \mathcal{L}_B + \lambda\mathcal{L}_{SB},\end{aligned} \tag{4.1}$$

where λ is the dimensionless coupling constant representing the strength of the noise. The evolution of density operator $\varrho(t)$, describing the system and the environment, is governed by the von Neumann–Liouville equation $\dot{\varrho}(t) = \mathcal{L}(t)\varrho(t)$. We assume that there are no initial correlations between system and bath (i.e., the initial state is factorized) and that the bath is in equilibrium (e.g., in a thermal state). The main hypothesis in the derivation of a master equation is that the typical timescale of the evolution is much slower than the timescales characterizing the bath. We shall also assume that the timescale related to the rate of change of the system Hamiltonian is the slowest timescale of our problem: this is clearly related to the adiabaticity of the evolution. In other words, compared to the bath correlation time, the evolution of $\mathcal{L}_S$ is always "adiabatic." This is assured by the condition

$$\tau_c\Delta \ll 1, \tag{4.2}$$

where τ_c is the correlation time of the bath and the energy gap $\Delta = \min|\epsilon_n(t) - \epsilon_m(t)|$ characterizes the rate of change of $\mathcal{L}_S$. Under these conditions, one gets

$$\dot{\sigma}(t) = [\mathcal{L}_S(t) + \lambda^2\Gamma(t)]\sigma(t), \tag{4.3}$$

where $\sigma(t) = \mathrm{Tr}_B\{\varrho(t)\}$ is the system density matrix and $\Gamma(t)$ is a time-dependent dissipation superoperator. Equation (4.3) is the same master equation one would obtain by considering $\mathcal{L}_S(t)$ "frozen" at time t and evaluating the decay rates and the frequency shifts at the instantaneous eigenfrequencies $\omega(t) = \epsilon_m(t) - \epsilon_n(t)$ of the system Liouvillian.

We now consider the physical system described in Section 3. For simplicity, let the environment affect only the transitions between levels $|0\rangle$ and $|e\rangle$; this is enough for our purposes. The total Hamiltonian is $H_T(t) = H(t) + H_B + \lambda H_{SB}$, where $H(t)$ is the system Hamiltonian. The bath is bosonic, $H_B = \sum_k \omega_k a_k^\dagger a_k$, where ω_k is the frequency of the kth mode. The interaction Hamiltonian is $H_{SB} = \sum_k \gamma_k(|0\rangle\langle e| + |e\rangle\langle 0|) \otimes (a_k^\dagger + a_k)$, where γ_k is the coupling constant between the system and the kth mode of the bath. By using Eq. (3.2) and the form of the interaction Hamiltonian, we can obtain time-dependent Lindblad operators describing the transitions caused by the environment. In the interaction picture generated by the operator R defined in (2. 1), the density operator $\sigma_R(t) = R^\dagger\sigma(t)R$ satisfies the following master equation:

$$\begin{aligned}\dot{\sigma}_R(t) = &-i[H_S(0), \sigma_R(t)] - i[D(t, 0), \sigma_R(t)] \\ &+ \lambda^2\Gamma(t)\sigma_R(t),\end{aligned} \tag{4.4}$$

where the Lamb shifts and the decay rates can be evaluated by standard formulas [14, 23] when one introduces the appropriate thermal spectral densities.

5. FIDELITY AND BEHAVIOR OF THE OPTIMAL WORKING POINT

Equation (4.4) was numerically integrated along the loop in Fig. 1b when the three arcs are covered at a constant angular speed. The values of the Lamb shifts and decay rates were assigned, somewhat arbitrarily, for illustrative purposes. They correspond to a bath at very high temperature.

The behavior of the average fidelity (3.4), with $\sigma(\Omega\tau, \vartheta, \varphi)$ numerically obtained from (4.4), is shown in Fig. 3: from top to bottom, the dissipation constant increases from $\lambda^2 = 0$ to 0.05. In the noiseless case (uppermost line), the fidelity tends to 1 when $\Omega\tau \longrightarrow \infty$ (adiabatic limit). This asymptotic value is not reached monotonically: there are some oscillations, with maxima at $F = 1$ in the noiseless case. This is the case discussed in Section 3: the NOT transformation is perfect, even though one is far from the adiabatic regime, at the time values given by (3.7).

Clearly, in the presence of noise, the fidelity decreases as the time needed for the transformation increases. This can make it difficult to obtain a pure geometrical transformation (because of the necessary adiabatic condition). Therefore, it appears convenient to take advantage of the presence of the peaks. As a matter of fact, the fidelity decrease due to the noise is very small in the nonadiabatic regime and one can think of realizing the NOT gate by fine tuning the total operation time. As the best performance is obtained for the first peak of the fidelity (*optimal operation point*), we shall focus on the λ dependence of the coordinates of the first significant maximum, F^* and τ^*, and their deviation from the noiseless values F_0^* and τ_1^* (see Fig. 2). It is important to stress that, in the nonadiabatic regime, the gate is no longer purely geometrical; in

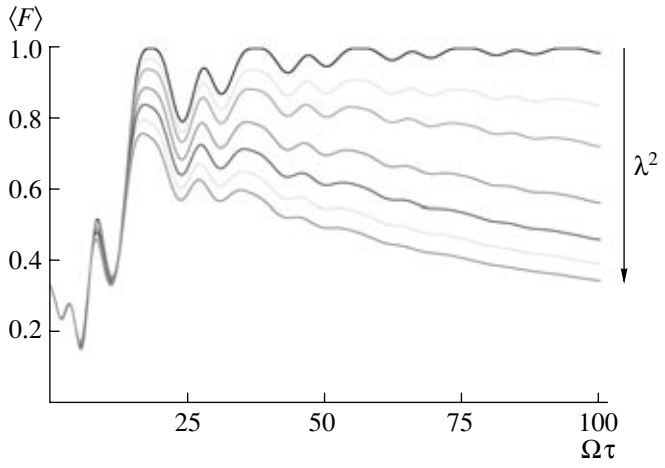

Fig. 3. Mean fidelity $\langle F \rangle$ versus cyclic time $\Omega\tau$. The dissipation constant λ^2 increases from top to bottom: $\lambda^2 = 0$ (noiseless case), 0.005, 0.01, 0.02, 0.03, 0.04, and 0.05.

principle, it would be possible to extract the geometric contribution, but one would not gain any additional information useful for experimental purposes.

A critical issue is the total amount of noise. In the simulations in Fig. 3, we considered a noise strength λ^2 ranging from 0.005 to 0.050. However, a realistic physical estimate, using thermal spectral densities, would yield a noise level below 0.005 [14]. In this regime, the fidelity at the optimal point reaches values greater than 0.9. From this result, it is clear that we can exploit the optimal times for realizing the NOT transformation with a relatively high fidelity even in the absence of additional control.

It is important to understand how the optimal time and the corresponding value of fidelity change by increasing the strength of the noise. This should yield information about the robustness of holonomic quantum computation against the detrimental effects of noise. Figure 4a shows the behavior of F^* for small noise: the points are the result of a numerical analysis and the continuous line is the fit

$$F^* = 1 - F_2\lambda^2, \tag{5.1}$$

yielding $F_2 = 6.34$. The agreement is excellent and enables one to conclude that fidelity decreases linearly with λ^2 for $\lambda^2 \le 10^{-3}$. The behavior of F^* for larger values of λ^2 is displayed in Fig. 4b. The fit is

$$F^* = 1 - F_2\lambda^2 + F_4\lambda^4, \tag{5.2}$$

with $F_4 = 29.93$. Observe that $\lambda^2 \simeq 6 \times 10^{-2}$ is a very large (unphysical) value. The conclusion that fidelity decreases as λ^2 (for small λ) is to be expected from a perturbation expansion of the master equation (4.4).

Let us now analyze the behavior of the optimal time τ^* vs. λ^2. Figure 5a displays the optimal time vs. λ^2 in the small-coupling case. The values of τ^* are more affected by errors due to the approximations introduced by the numerical calculations. The optimal time decreases by increasing λ^2. The fit yields

$$\tau^* = \tau_1^* - \tau_2\lambda^2, \tag{5.3}$$

with $\tau_2 = 59.40\Omega^{-1}$, the value $\tau_1^* = 18.25\Omega^{-1}$ being obtained analytically from Eq (3.8). Again, the linear fit is in good agreement with the data and enables one to conclude that the optimal time decreases linearly with λ^2 for $\lambda^2 \le 10^{-3}$. The behavior of τ^* for larger values of λ^2 is displayed in Fig. 5b. In this case, the fit is

$$\tau^* = \tau_1^* - \tau_2\lambda^2 + \tau_4\lambda^4 - \tau_6\lambda^6, \tag{5.4}$$

with $\tau_4 = 990.65\ \Omega^{-1}$ and $\tau_6 = 7655.95\ \Omega^{-1}$.

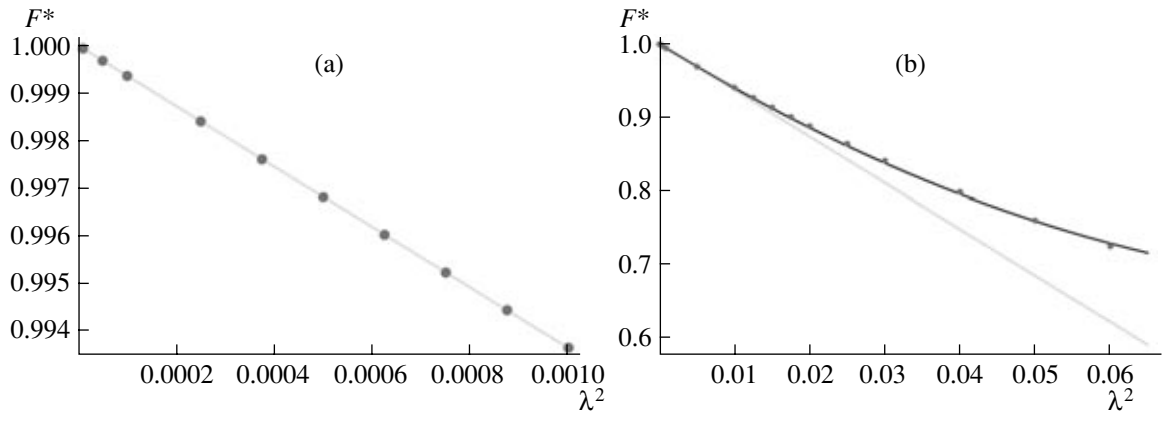

Fig. 4. Maximum value of the mean fidelity F^* vs. noise (coupling to the bath) λ^2. (a) Small coupling: the fit yields $F^* = 1.00 - 6.34\lambda^2$. (b) Larger coupling: the fit yields $F^* = 1.00 - 6.34\lambda^2 + 29.93\lambda^4$; linear fit as in (a). The error bars are always smaller than the size of the points.

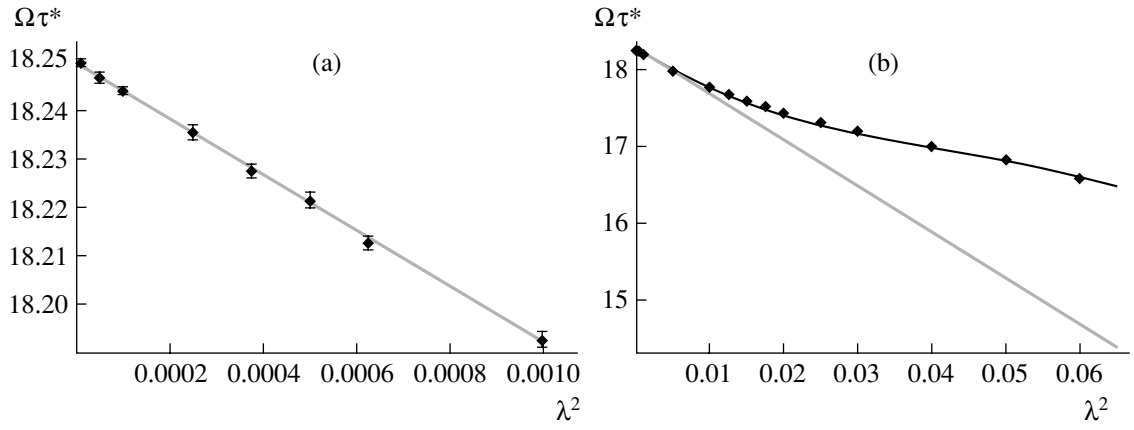

Fig. 5. Optimal time τ^* vs. noise (coupling to the bath) λ^2. The values of τ^* are more affected by error than those of F^*. (a) Small coupling: the fit yields $\Omega\tau^* = \Omega\tau_1^* - 59.40\lambda^2$, with $\Omega\tau_1^* = 18.25$, the theoretical value (3.8). (b) Larger coupling: the fit yields $\Omega\tau^* = \Omega\tau_1^* - 59.40\lambda^2 + 990.65\lambda^4 - 7655.95\lambda^6$; linear fit as in (a).

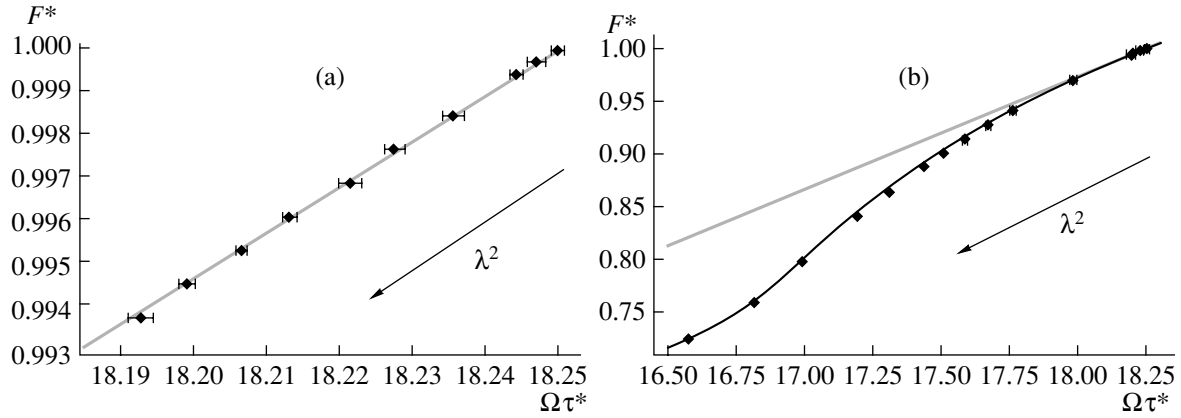

Fig. 6. Maximum value of the mean fidelity vs. the optimal working time τ^*. (a) Small coupling: the fit yields $F^* = 1.00 + 0.11\Omega(\tau^* - \tau_1^*)$. (b) Larger coupling; the errors are included in the size of the points and the linear fit is as in (a).

The behavior of the point (F^*, τ^*) is shown in Fig. 6, both for small (Fig. 6a) and larger (Fig. 6b) values of λ^2. From Eqs. (5.1) and (5.3), one obtains

$$F^* = 1 - \frac{F_2}{\Omega\tau_2}\Omega(\tau_1^* - \tau^*) = 1.00 + 0.11\Omega(\tau^* - \tau_1^*). \quad (5.5)$$

This is the small-coupling situation displayed in Fig. 6a. Notice that the mean fidelity increases linearly with τ^* in this regime. In the presence of noise, optimal quantum gates are less precise and slightly faster than the ideal ones. A further analysis of this dependence for larger values of the noise (using Eqs. (5.2) and (5.4)) yields an involved algebraic expression that includes higher order corrections. The behavior is shown in Fig. 6b. The evolution of the optimal working point is summarized in Fig. 7.

6. ROBUSTNESS AND CONCLUSIONS

In order to shed some light on the robustness of the quantum gate in the neighborhood of the optimal working point, it is useful to compare the optimal fidelity F^* with the fidelity obtained in the adiabatic limit F_{adiab}. Let us observe that, in general, the analysis of decoherence in geometric computation raises a critical issue in connection with adiabatic evolutions, which cannot be too slow, as decoherence would eventually destroy any

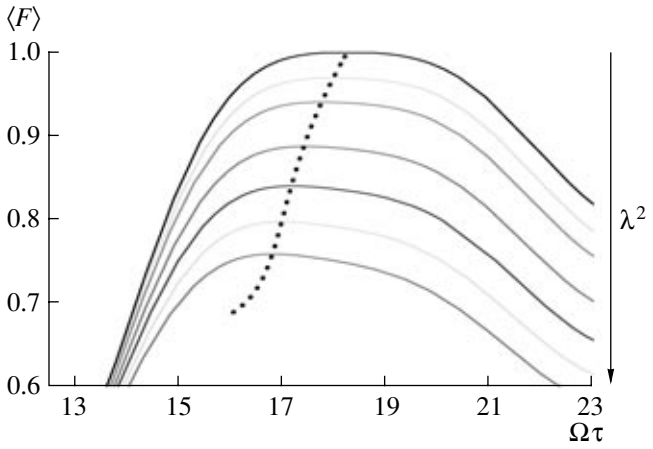

Fig. 7. Mean fidelity $\langle F \rangle$ versus cyclic time $\Omega\tau$: a closer look at the evolution of the optimal point in Fig. 3. The dissipation constant λ^2 increases from top to bottom: $\lambda^2 = 0$ (noiseless case), 0.005, 0.01, 0.02, 0.03, 0.04, and 0.05. The dotted line is the fit described in the text.

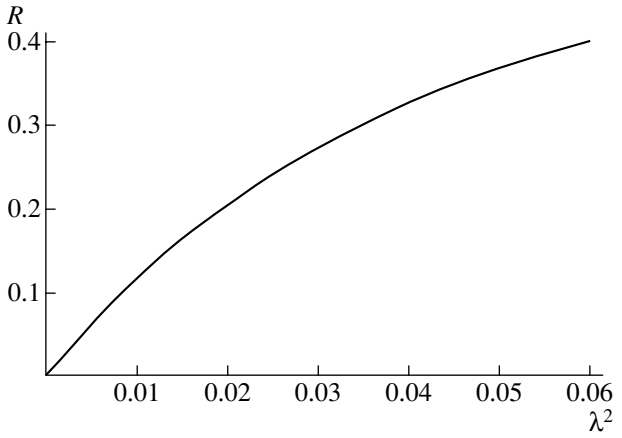

Fig. 8. Robustness parameter R vs. λ^2.

interference. This inevitably introduces an element of arbitrariness in the following definitions.

We shall evaluate the performance of the optimal (nonadiabatic) quantum gate, as compared to its adiabatic limit, through a "robustness" parameter:

$$R = \frac{F^* - F_{\text{adiab}}}{F^*}. \tag{6.1}$$

By glancing at Figs. 2 and 3, it is apparent that the adiabatic limit is practically attained already at the third peak, namely, for $\tau = \tau_3^*$ in Eq. (3.7). We therefore take

$$F_{\text{adiab}} \simeq F(\Omega\tau_3^*) = F\left(\frac{3\pi}{2}\sqrt{143}\right). \tag{6.2}$$

The dependence of R on λ^2 is displayed in Fig. 8. Clearly, the (relative) robustness of the optimal gate is larger for larger noise levels. We notice the presence of a linear regime for small coupling.

Although we focused our attention on the particular physical system shown in Fig. 1a, our conclusions are rather general and are valid for other physically relevant situations. There exist some values of the duration of the evolution for which the fidelity is 1, even though this is far from the adiabatic regime. As already emphasized at the end of Section 3, these results can be extended to more general loops, yielding optimal times as in Eq. (3.9).

The presence of these optimal peaks is important for experimental applications: if the total operation time can be tuned to the first peak, one can realize a transformation that is the most robust against noise. Moreover, the maximum value of the fidelity exhibits different regimes: for small coupling, it decreases linearly with λ^2. In general, the gate can be considered robust when compared to the standard adiabatic one. This can be of interest for experimental applications if one aims to introduce further control. The case of two-qubit gates is not trivial and is at present under investigation.

ACKNOWLEDGMENTS

This work was supported in part by the European Community through the Integrated Project EuroSQIP and by the bilateral Italian–Japanese Projects II04C1AF4E on Quantum Information, Computation, and Communication of the Italian Ministry of Instruction, University, and Research.

REFERENCES

1. *Geometric Phases in Physics*, Ed. by A. Shapere and F. Wilczek (World Sci., Singapore, 1989).
2. A. Bohm, A. Mostafazadeh, H. Koizumi, et al., *The Geometric Phase in Quantum Systems* (Springer, 2003).
3. M. A. Nielsen and I. L. Chuang, *Quantum Computation and Quantum Information* (Cambridge Univ. Press, Cambridge, 2000).
4. G. Benenti, G. Casati, and G. Strini, *Principles of Quantum Computation and Information* (World Sci., Singapore, 2004).
5. J. A. Jones, V. Vedral, A. Ekert, and G. Castagnoli, Nature **403**, 869 (2000); A. Ekert, M. Ericsson, P. Hayden, et al., J. Mod. Opt. **47**, 2501 (2000).
6. P. Zanardi and M. Rasetti, Phys. Lett. A **264**, 94 (1999); J. Pachos and P. Zanardi, Int. J. Mod. Phys. B **15**, 1257 (2001).
7. L. M. Duan, J. I. Cirac, and P. Zoller, Science **292**, 1695 (2001).
8. G. Falci, R. Fazio, G. M. Palma, et al., Nature **407**, 355 (2000).
9. L. Faoro, J. Siewert, and R. Fazio, Phys. Rev. Lett. **90**, 028301 (2003).

10. P. Solinas, P. Zanardi, N. Zanghì, and F. Rossi, Phys. Rev. A **67**, 062315 (2003).
11. D. Giulini, E. Joos, C. Kiefer, et al., *Decoherence and the Appearance of a Classical World in Quantum Theory* (Springer, Berlin, 1996).
12. P. Solinas, P. Zanardi, and N. Zanghì, Phys. Rev. A **70**, 042316 (2004).
13. I. Fuentes-Guridi, F. Girelli, and E. R. Livine, Phys. Rev. Lett. **94**, 020503 (2005).
14. G. Florio, P. Facchi, R. Fazio, et al., Phys. Rev. A **73**, 022327 (2006).
15. D. Parodi, M. Sassetti, P. Solinas, et al., quant-ph/0510056.
16. M.S. Sarandy and D.A. Lidar, Phys. Rev. A **73**, 062101 (2006).
17. Y. Aharonov and J. Anandan, Phys. Rev. Lett. **58**, 1593 (1987).
18. J. Anandan, Phys. Lett. A **133**, 171 (1988).
19. M. V. Berry, Proc. R. Soc. London, Ser. A **392**, 45 (1984).
20. F. Wilczeck and A. Zee, Phys. Rev. Lett. **52**, 2111 (1984); A. Zee, Phys. Rev. A **38**, 1 (1988).
21. C. W. Gardiner and P. Zoller, *Quantum Noise*, 2nd ed. (Springer, Berlin, 2000).
22. E. B. Davies and H. Spohn, J. Stat. Phys. **19**, 511 (1978).
23. P. Facchi, S. Tasaki, S. Pascazio, et al., Phys. Rev. A **71**, 022302 (2005).